ACS APPLIED MATERIALS & INTERFACES

Research Article

www.acsami.org

Heat Treatments Modify the Tribological Properties of Nickel Boron Coatings

Kevin L. Gilley,[†] Juan C. Nino,[†] Yancy W. Riddle,[‡] David W. Hahn,[§] and Scott S. Perry*[,†]

[†]Materials Science and Engineering, University of Florida, Gainesville, Florida 32611, United States

[‡]Diamond Materials Tech, Inc., Colorado Springs, Colorado 80907, United States

[§]Mechanical and Aerospace Engineering, University of Florida, Gainesville, Florida 32611, United States

ABSTRACT: The effects of annealing temperature on the tribological properties of electroless nickel−boron coatings have been investigated. The coatings were annealed in a tube furnace under a flow (0.0094 N m^3/min) of oxygen gas at temperatures of 250, 400, 550, and 700 °C for 3 h. Using scanning electron microscopy, images of the annealed coatings documented changes in surface morphology. From this it was seen that the higher annealing temperatures produced marked changes, moving from the nodular structure of nickel−boron coatings to a flaked surface morphology. The chemical effect of the annealing temperature was studied via X-ray photoelectron spectroscopy (XPS) and Raman spectroscopy. The XPS data indicated that after annealing at the temperatures of 550 and 700 °C, an accumulation of boron oxide species could be seen at the surface as well as a complete loss of nickel signal. An analysis of Raman spectra collected across the surface further identified the predominant species to be boric acid. The tribological response of the coatings was studied with a pin-on-disk tribometer with 440C stainless steel balls run against the coatings in ambient air. It was seen that the as received sample and the sample annealed at 250 °C samples exhibited modest friction properties, while the 400 °C sample had increased friction due to wear debris from the ball. The 550 and 700 °C samples showed remarkably low friction coefficients between 0.06 and 0.08, attributable to the presence of boric acid. The wear tracks were analyzed using scanning white light interferometry and from this data wear rates were obtained for the coatings ranging from 10^{-8} to 10^{-7} mm^3/Nm.

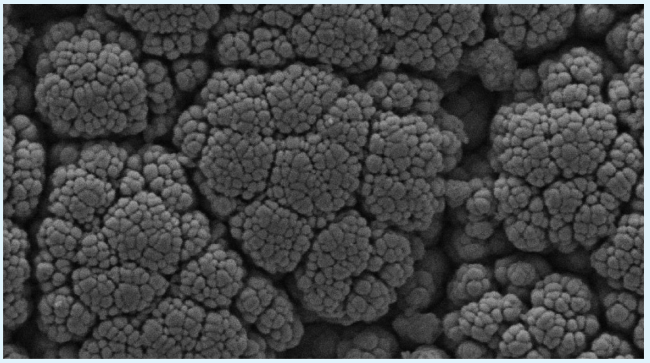

KEYWORDS: *nickel boron, low friction coating, electrolessly deposited coating, low wear coating, tribology, boric acid*

1. INTRODUCTION

There is a large need in the design of engineered pieces for the protection and enhancement of the performance of surfaces. In 2009, the global coatings market totaled over $90 billion USD with nondecorative coatings (such as marine, hard coatings, and tribological coatings) making up over 50% of the market.[1] Hard coatings such as diamond-like carbon, chrome coatings, and boron nitride are commonly used to increase the hardness of a surface to prolong its operation. By covering the surface with a hard coating the lifetime of the part is increased due to the fact that the piece will experience less wear during operation. Hard coatings can also modify other properties of the surface, potentially providing resistance to corrosion, improved frictional behavior, and protection from unwanted chemical reactions. Nickel boride coatings offer a number of these advantages.[2−7]

A number of coating processes can be used to deposit nickel boride, including physical vapor deposition, chemical vapor deposition, and electrolytic deposition. One of the increasingly used deposition processes is electroless deposition. Electroless deposition is a purely catalytic process in which no external power source is needed to drive the deposition. Also electroless deposition eliminates line-of-sight issues as well as edge effects commonly seen in many deposition processes.[8] Advantages of this approach also include the relative simplicity in equipment, low capital expenditure, scalability, and the overall lower workforce skill involved in the deposition.[8−10] The electroless deposition of nickel boron coatings is beneficial in protecting against corrosion and fouling, extending of service lifetimes, and conservation of energy. Nickel boron coatings have been shown in previous studies to have high hardness, low wear, good adherence on a variety of substrates, and provide corrosion resistance.[10] In certain situations, nickel boron coatings have shown low friction but many factors such as deposition variables, annealing temperature, and tribological testing environment play a large role in the variance on friction values reported.[11,12] Nickel boron coatings are commonly annealed under ambient gas conditions to increase the hardness of the coatings; 400 °C is commonly used as a result of empirical investigations that revealed an enhancement in hardness

Received: March 10, 2012
Accepted: May 29, 2012
Published: May 29, 2012

following this treatment.[13,14] In the present study, the influence of temperature-dependent oxygen anneals on the tribological properties of electroless nickel boride coatings have been investigated in order to elucidate the various contributions to the modified coating properties.

Following anneals under a flow of oxygen gas at 250, 400, 550, and 700 °C, X-ray photoelectron spectroscopy (XPS) has been used to document the composition of nickel boride coating surfaces as a function of annealing temperature. In addition, Raman spectroscopy has assisted in ascertaining the molecular nature of the boron oxide species detected in the near surface region following high temperature anneals. In turn, compositional changes have been correlated with variations in surface morphology and tribological response in order to generate a thorough understanding of the origins of favorable performance characteristics. Pin-on-disk tribometry has been used to measure the friction and associated wear properties of the nickel boride coatings as a function of annealing treatments.[18] The pin-on-disk measurements have provided an average coefficient of friction for a given set of sliding conditions while interferometry measurements have been used to follow the amount of material lost during sliding. Using known variables from the pin-on-disk testing, fundamental wear rates of the variously annealed coatings have been obtained.

2. METHOD AND MATERIALS

Numerous 4130 steel substrates measuring approximately 10 mm × 14 mm were processed by UCT Coatings Inc. (Stuart, FL) to deposit a 100 μm thick nickel−boron coating from a nickel chloride hexahydrate (NiCl2·6H2O) and sodium borohydride ($NaBH_4$) solution. Lead tungstate ($PbWO_4$) was employed as a solution stabilizer. The coating thickness was monitored via deposition rate calculations and verified via cross-sectional SEM images.

A tube furnace allowed for ultrahigh purity O_2 gas to be flowed over the coated substrates during the various annealing procedures. A steady flow of 0.0094 N m^3/min was established to purge the tube of any ambient air before heating to the specified temperature. Temperature was measured via a K-type thermocouple placed inside the tube immediately above the sample. Once the desired temperature was reached, the samples were held at this temperature for 3 h. Samples were allowed to cool to room temperature under a flow of O_2 gas.

XPS was performed with an Omicron Nanotechnology GmbH Al Kα (1486.7 eV) monochromatic X-ray source, used in conjunction with an Omicron Nanotechnology GmbH EAC2000-Sphera hemispherical, 7-channel analyzer. After annealed samples were attached to transfer platens via spot-welded Ta strips, low resolution survey spectra were taken for the 1386.7−50 eV binding energy range to identify the elements present in the surface region of the coatings. High resolution core spectra were measured for the elements present to determine the chemical bonding state of the elements present and to calculate their relative concentration within the selvage region. A takeoff angle of 55°, a spot size of 1750 × 2750 μm, and a spectral step size of 0.03 eV within core scans were employed. All samples were sputtered for 5 min with a PHI FIG-5CE ion sputter gun with beam energy of 1 kV before general survey spectra were taken to remove surface contamination. Processing of the XPS spectra was performed using CasaXPS software (Casa Software Ltd.) and entailed a sequence of background subtraction, curve fitting, integration of peak intensities, and correction for each element's atomic sensitivity factor.[15−17] The Shirley background subtraction method was used to subtract the background intensity for the spectra and a 30% Lorentzian/70% Gaussian profile was used in fitting core level peaks.

Raman spectra were collected with a LabRam Infinity (Horiba Group) micro-Raman system, employing 1.5 mW continuous helium: neon laser (λ = 632.8 nm) and a 100× objective. Spectra were recorded using 6 s integration times and averaged 10 times for a total integration time of 60 s. Backscattered radiation was collected by the same microscope objective, passed through a sharp-edge filter to reject elastically scattered light, and imaged by a CCD detector (1024 9 256 pixels).

Tribological testing was performed via a novel ultrahigh vacuum tribometer, seen in (Figure 1), which was based on the MISSE 7 series of pin-on-disk tribometers transported to the International Space Station (ISS) and installed in November 2009 during the STS 129 mission.[19]

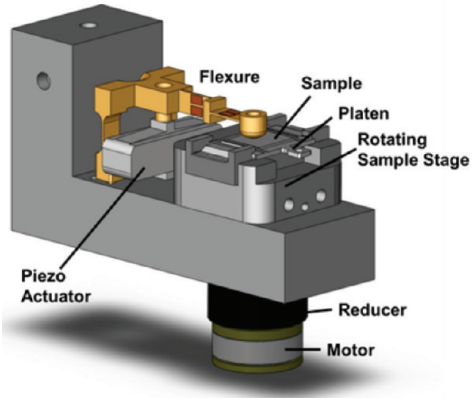

Figure 1. Schematic of the home-built pin-on-disk tribometer wear track radius of 18.85 mm and a piezoelectric controlled flexure arm. Stage is capable of rotating up to 30 rpm and holds samples mounted to Omicron GmbH platens.

The full design details and specifics of the tribometer have been previously reported in the literature.[20] All samples were run against a 3 mm radius 440C stainless steel ball under ambient conditions with a relative humidity of 40−50%. The tribological investigations entailed the application of 1 N normal load and sliding distances in excess of 1 km. Under these conditions, the estimated contact pressure of the sliding interface was 530 MPa, calculated assuming a Hertzian contact; higher local pressures likely existed in the region of asperities.

Scanning white light interferometry (SWLI) scans were taken using a Veeco Wyko NT9100 Interferometer. Scans over multiple regions were processed and compiled in order to illustrate broad regions including the wear track. Single point wear rates (K) were calculated for each sample according to the following relationship

$$K = \frac{V}{(F_n d)} \ (\mathrm{m}^3/\mathrm{N\text{-}m}) \quad (1)$$

where normal load is denoted by F_n, total sliding distance by d, and volume loss by V. Multiple measurements across the wear tracks were acquired and analyzed to establish an average wear track shape and standard deviations in wear rates for each of the samples.

SEM images were obtained using a JEOL NeoScope JCM-5000 benchtop SEM employing a primary beam energy of 10 kV. Images were obtained from the region of the wear track of each sample to illustrate the deformation and damage caused by the tribological tests. Images were also obtained off of the wear track to depict the general morphology of the coating and to document changes occurring as a result of the annealing processes. The surface hardness values of the nickel boride coatings were evaluated with a Hysitron Triboindeter, employing a three-sided Berkovich diamond indenter.

3. RESULTS

3.1. Compositional and Morphological Changes.

Figure 2 shows SEM images of the undisturbed portions of the coatings not affected by the tribological testing performed. The as received sample along with the sample annealed at 250 °C depict a nodular structure for the nickel−boron coatings. In the 400 °C annealed sample aggregation on the submicrometer

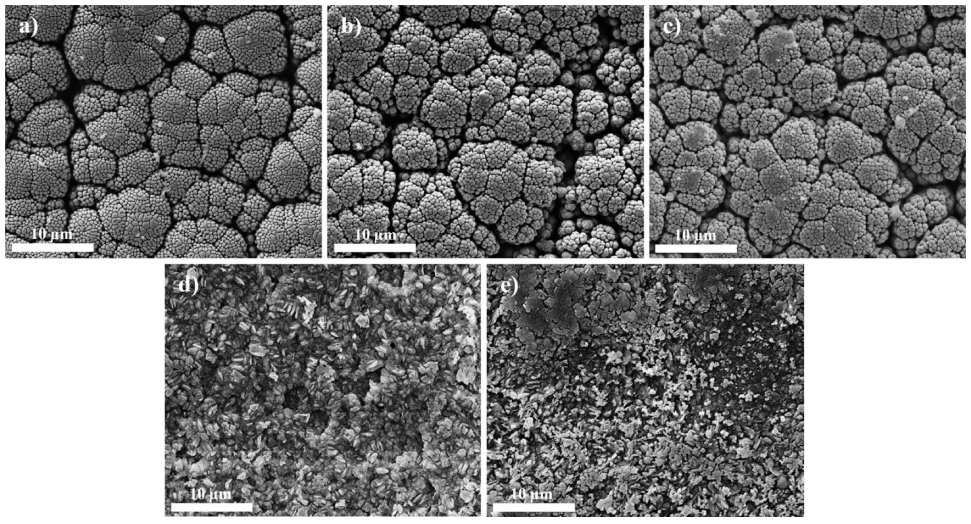

Figure 2. SEM Images of the surface of the NiB coatings (a) as received and after annealing at (b) 250 °C, (c) 400 °C, (d) 550 °C, and (e) 700 °C showing the morphological changes that occur due to the annealing at these temperature.

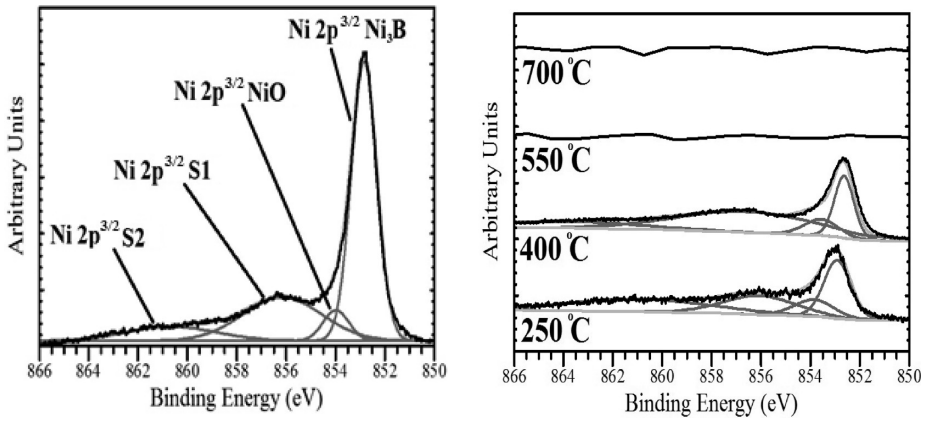

Figure 3. Ni 2p 3/2 core spectra showing that after higher annealing temperatures no Ni is seen in the sample's surface region.

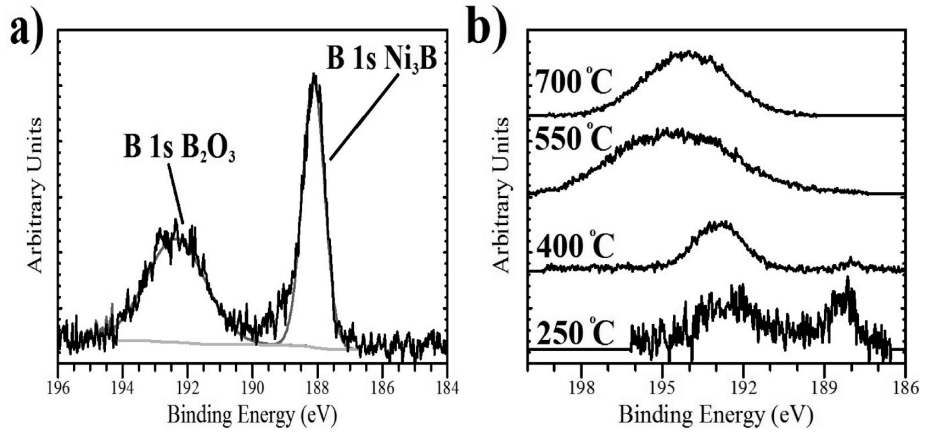

Figure 4. B 1s core spectra showing (a) the fitted as received sample with peak assignments and (b) the spectra for the 250 °C, 400 °C, 550 °C, and 700 °C samples showing a transition from 2 peaks in the lower annealed samples to a singular broad peak in the higher annealed samples.

scaled is observed upon close inspection in the form of smaller nodules coalescing, smaller surface cracks closing, and deeper cracks appearing less prevalent. Upon annealing at 550 °C extensive changes can be seen in the morphology. The nodular structure is completely absent, replaced by a new phase on the surface. This new structure, dubbed hereafter as flaked, can also be seen in the sample annealed at 700 °C. Also seen in the 700 °C image are slight remnants of the nodular structure indicating that the new flaked structure has evolved from the previous structure.

Figure 3 depicts the Ni 2p 3/2 core spectra for the series of coatings annealed. The Ni 2p spectrum is notoriously difficult

dx.doi.org/10.1021/am3004297 | ACS Appl. Mater. Interfaces 2012, 4, 3069−3076

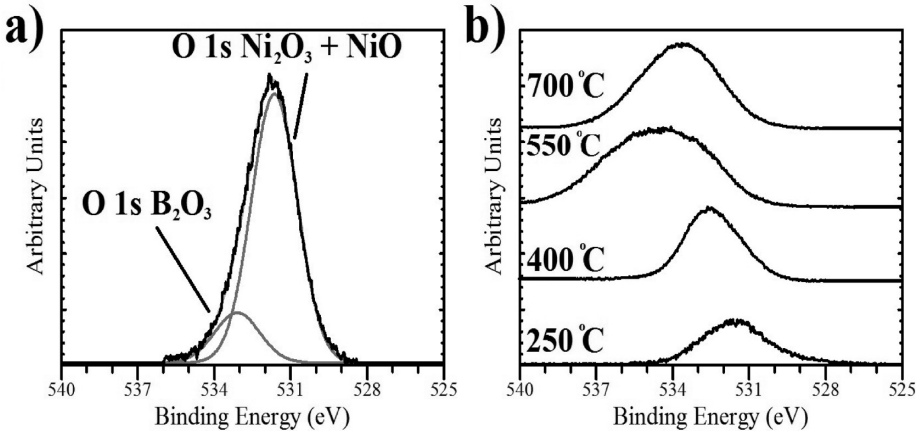

Figure 5. O 1s core spectra (a) showing peak identification for the as received sample and (b) remaining samples O 1s spectra showing transition in binding energy and broadening of the peak due to the creation of a B_2O_3 rich surface in the higher annealed samples.

to fit due to the number of satellite peaks, denoted in the spectra as S1 and S2, which occur due to quantum mechanical effects.[21] Despite these complexities, the 2p 3/2 peak can be fitted with two smaller peaks. The first peak located at approximately 853 eV is associated with Ni bonded to B in the compound Ni_3B, the intended stoichiometric compound during deposition. Prior experiments have shown that as nickel−boron coatings are annealed, the films crystallize and the dominant phase seen is Ni_3B.[2] The second fitted peak, located at 853−854 eV, is assigned to Ni bonded to O in the compound NiO. An additional nickel oxide, Ni_2O_3, may potentially form with a characteristic Ni binding energy of 856−857 eV. Unfortunately this peak overlaps with one of the satellite peaks and therefore cannot be fully assessed. Slight variations in the intensity of these spectral features are seen in the as-received sample and those annealed to 250 and 400 °C, however the complete absence of any Ni species is indicated by the spectra measured from samples annealed to 550 and 700 °C. Based on these results, lower annealing temperatures are seen to produce a minor oxidation of the nickel boron coating, while higher temperature anneals are seen to induce a drastic compositional change to the surface region, consistent with the morphological changes described above.

Figure 4 displays the B 1s core spectra for the samples annealed to different temperatures in the study. The relative decrease in the signal-to-noise ratio (S/N) compared to the Ni spectra results from the lower photoelectron cross section for boron. As can be seen in the as received, 250 °C, and 400 °C samples there are two peaks expressed. The lower binding energy peak is located at approximately 188 eV and corresponds to boron bonded to Ni in the Ni_3B structure. The higher peak, located at approximately 193 eV can be assigned to B bonded to O. This shows that even in the as deposited coating some degree of surface oxidation has occurred. In the samples annealed at the higher temperatures, the lower binding energy peak is no longer seen and a single broad peak is observed. This peak is attributed to boron oxide species and/or boric acid resulting from the diffusion of subsurface boron and hydrogen at these temperatures and the extensive oxidation of the surface region. The proximity of reported binding energies for B_2O_3 (193.7 eV) and H_3BO_3 (192.8 eV)[22] and the ill-defined shape of the spectral peak prevent a quantitative deconvolution into their respective presence. The formation of hydrogen containing boric acid is consistent with the inclusion of hydrogen in Ni_3B films produced through electroless deposition. The breadth of the peak and the shift to higher energies is also observed for both oxygen and adventitious carbon detected in related spectra and is consistent with surface charging of the oxide. These spectral features observed with increasing temperature demonstrate that all of the boron present in the near surface region is converted from its deposited form (Ni_3B).

Figure 5 displays the correlated changes observed in the O 1s peak as the annealing temperature increases. The lower annealed samples and the as received sample show a peak that can be assigned as arising from two species. Intensity located at approximately 532 and 533 eV and can be attributed to Ni_2O_3 and B_2O_3, respectively. For the sample annealed to 250 °C, deconvolution of the O 1s peak reveals intensity at 529 eV that can be attributed to NiO in addition to that observed for the as received sample. Upon annealing to 400 °C, a relative shift in intensity located at 533 is consistent with the formation of more boron oxide species. After annealing above 550 °C, the O 1s peak shifts to a higher binding energy and widens much like the case in the B 1s peak, consistent with the complete oxidation of the surface region and related surface charging.

From the spectra above, the relative percent composition of the surface of the coatings was determined using the methods previously described and are presented as atomic percentages in Table 1. As XPS is insensitive to the presence of hydrogen, its relative presence in the near surface region is not reflected. The data for the samples annealed to 250 and 400 °C indicate that a change in surface composition has occurred as a result of the heat treatment. The presence of C in all of the samples can be attributed to adventitious carbon that adsorbs to the surface of the sample during transport from the tube furnace to the vacuum system. In the electroless deposition process, $PbWO_4$ is used, in very minute quantities, as a stabilizer for the

Table 1. Elemental Composition, in Atomic Percent, of the Samples after Annealing at Various Temperatures

sample	Ni (at. %)	B (at. %)	O (at. %)	C (at. %)	Pb (at. %)
as received	31	19	42	8	0
250 °C	22	23	45	10	0
400 °C	24	24	45	6	1
550 °C	0	34	49	17	0
700 °C	0	32	53	15	0

dx.doi.org/10.1021/am3004297 | ACS Appl. Mater. Interfaces 2012, 4, 3069−3076

bath.[13,14,23,24] In some samples, a small amount of Pb has been detected on the surface, usually less than or equal to one atomic percent, as seen in the 400 °C composition data. The samples annealed to 250 and 400 °C exhibit a slightly higher B concentration at the cost of lower Ni concentration with respect to the as received coating. Significant changes in the composition occur once the coatings are annealed at 550 and 700 °C. For these samples, a complete depletion of nickel and higher concentrations of B and O with a much higher concentration of C is measured. The observed change in composition correlated closely with a significant reduction in surface hardness from ~3 GPa for coatings containing nickel and boron in the surface region to ~50 MPa for those containing predominantly boron and oxygen. The extent to which surface roughness influenced these values derived from nanoindentation measurements was not evaluated.

To further ascertain the nature of compositional changes occurring with high temperature anneals in oxygen environments, Raman spectra were collected from the Ni_3B coating annealed to 700 °C. The resulting spectrum is presented in Figure 6 and is consistent with the transformation of the near

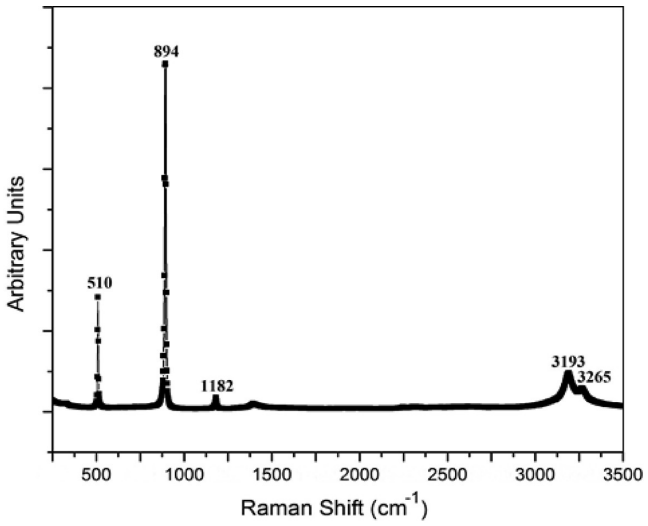

Figure 6. Raman spectrum of the electroless Ni_3B sample following a 700 °C anneal in a blanketing oxygen gas. The spectrum is dominated by vibrational peaks attributable to boric acid.

surface region to boric acid, H_3BO_3. The peaks at 510, 894, and 1182 cm^{-1} are in agreement with features previously assigned to boric acid.[25,26] In addition, the absence of peaks at 808, 1325, and 1475 cm^{-1} characteristic of B_2O_3 is noted.[27,28] The small feature at 1386 cm^{-1} in the spectrum reported here has not been assigned, nor were assignments for the features at 3193 or 3265 cm^{-1} identified through an extensive search of the literature. Nonetheless, the Raman spectrum clearly highlights the formation of boric acid and the influence of hydrogen incorporated into the film during deposition.

3.2. Friction Behavior. Figure 7 plots the coefficient of friction (μ) vs sliding distance (m) for each of the samples tested. As previously stated, the normal force in each test was 1N and the counterface was a 3 mm radius 440C stainless steel ball, resulting in an estimated contact pressure of 530 MPa. Again, a new counterface was employed for each unique sample. The as received and 250 °C samples behaved similarly, with each test having a run-in period for the first 100 m or so of sliding then holding at a value of around 0.5 for a period of 400

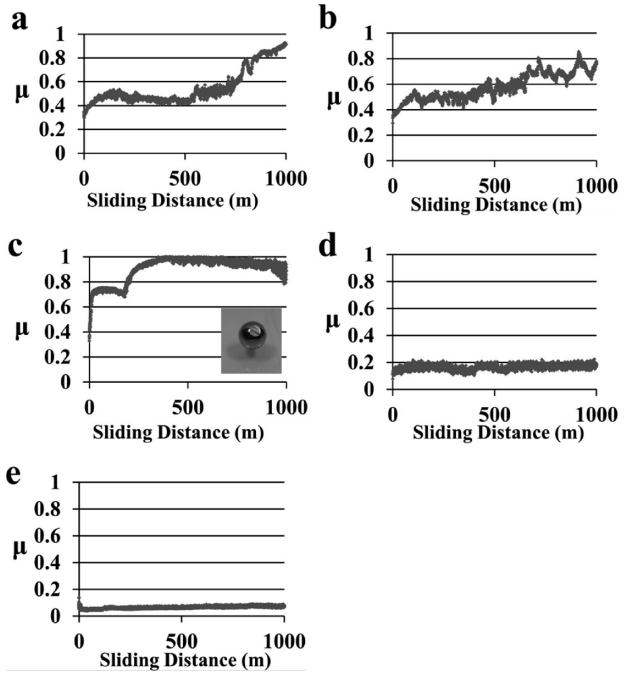

Figure 7. Friction coefficient vs sliding distance for Ni–B coatings (a) as received and after annealing at (b) 250, (c) 400, with inset picture of SS ball to show evidence of wear on the ball, (d) 550, and (e) 700 °C.

m. Then following ~600 m of sliding distance both samples exhibit a steady increase in μ until the end of the test, by which point the samples have reached coefficient of friction values of ~0.8–0.9. The frictional response of the 400 °C sample, (c), differs from the previous two samples. In the first 30 m of sliding, it begins with a sharp increase of the μ value from 0.35 to 0.7 and then holds steady at this higher value for the next 170 m of sliding. Then, a second, abrupt increase in μ occurs, increasing to a coefficient value of 1.0 for the remainder of the test. As will be discussed below, this second increase can be attributed to formation of wear debris within the wear track. Figure 6d and 6e illustrate a very different frictional response for the coatings annealed in oxygen to 550 and 700 °C. The 550 °C sample has a very brief run in period then holds at a value of approximately 0.15 for the duration of the test. The 700 °C sample starts at a slightly higher friction value then decreases to a steady state value of 0.06 for the remainder of 1 km sliding test.

3.3. Wear Behavior. The wear rates associated with the 1 km sliding runs were determined from an analysis of the circular wear tracks measuring 18.85 mm in circumference. Using line scans generated from SWLI and averaged over an entire image, the volume removed from the coating can be determined and from there the wear rate of the coating can be calculated. A representative section of an image analyzed in this way is shown in Figure 8, illustrating the well-defined wear track observed on the sample annealed to 550 °C. The wear rates of all 5 samples are shown in Table 2 as well as the average μ value over the entire test for each sample. The as received sample and 250 °C sample exhibit similar behavior having both average μ values and wear rates that are very close together. No wear rate could be calculated for the 400 °C sample due to debris accumulating on the surface, which will be discussed in greater detail later. The 550 and 700 °C samples exhibit a higher wear rate as compared to the lower annealed

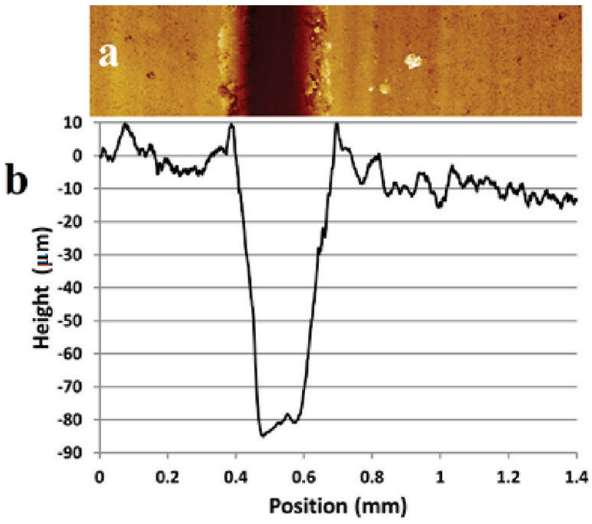

Figure 8. (a) SWLI image showing the wear track generated on the 550 °C sample. (b) Line plot of SWLI data, averaged over the entire area of the image, indicating the depth of the wear track.

Table 2. Coefficient of Friction and Wear Rates of All Samples Tested

sample	coefficient of friction	wear rate (mm^3/Nm)
as received	0.55	4.3×10^{-8}
250 °C	0.58	4.8×10^{-8}
400 °C	0.90	N/A
550 °C	0.17	2.7×10^{-7}
700 °C	0.06	2.1×10^{-7}

samples, although having lower coefficients of friction. The difference between the wear rates of the lower and higher annealed samples can be attributed to the change in both composition and morphology occurring over this temperature range, as described above. Overall, these wear rate values represent a very low rate of material removal from the contact zone as compared to many other materials coatings.[29,30]

The SWLI measurements further revealed the depth of wear tracks for the lower annealed samples to be between 10 and 30 nm. In comparison, some of the features on the surface resulting from deposition of the coatings are on the order of 5–15 nm. As a result, there appears to be more of a smoothing of the nodular structure than material removal. This smoothing effect can be seen in the as received and 250 °C samples SEM images shown in Figure 9a and b. Some of the thinner, deeper lines seen in the images arise from wear debris from the ball. The 400 °C sample shows a much broader wear track than the other samples as a result of the large flat spot formed on the ball during the testing, which lead to a larger contact area. The 550 and 700 °C samples, which displayed higher wear rates were revealed to have wear track depths between 70 and 120 nm. While this is much more than the lower temperature annealed samples, a removal of 100 nm correlates to 1/1000 of the 100 μm thick coating being removed in 1 km of sliding. As seen in Figure 9, the higher annealed samples do not display the smoothing effect seen in the as received and 250 °C samples, but exhibit a more typical material removal process within the wear track. The origin of the wider wear track observed on 700 °C sample (Figure 9e) has not been determined in these studies.

4. DISCUSSION

4.1. Compositional and Morphological Changes. As seen in the data presented above, the result of annealing Ni–B coatings in oxygen at temperatures of 550 °C and above is a marked change in both morphology and composition. These changes in turn lead to notable changes in the measured tribological properties. The typical nodular structure observed on the as received sample and following anneals up to 400 °C is converted to a flaked structure when coatings are subjected to higher annealing temperatures. The resulting coating morphology is smoother than the original coating surface, free of the cracks and gaps between nodules in the nodular structure. This change in surface morphology points to a complete change in the material that makes up the surface region of the coating.

This hypothesis is corroborated by the trends seen in the composition of the near surface region of the coatings determined via XPS. The as received sample and those annealed at lower temperatures have similar compositions showing both Ni and B in the selvage region. The B 1s core spectra indicate B bonded to Ni in Ni_3B as well as B bonded to O in B_2O_3 like species. Although the core spectra are consistent

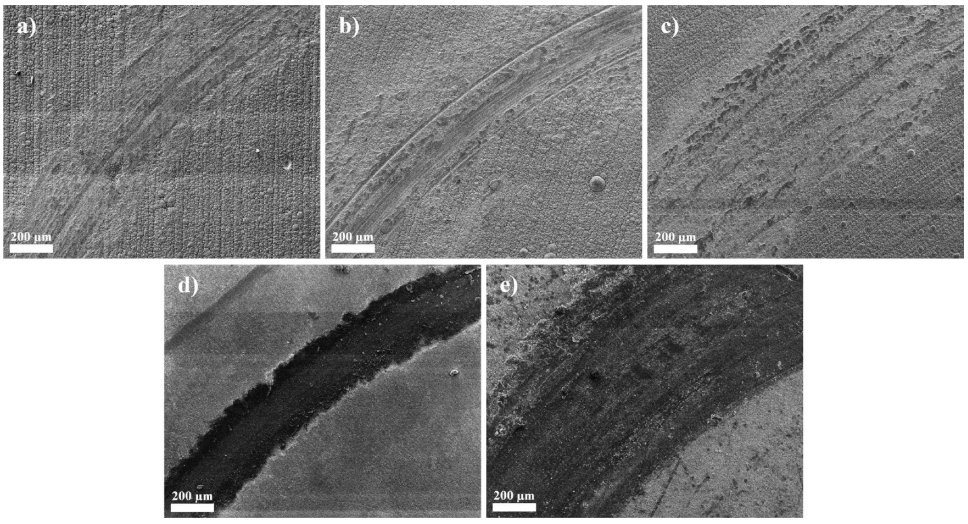

Figure 9. SEM images of wear tracks of NiB coatings for the (a) as received sample and after annealing at (b) 250, (c) 400, (d) 550, and (e) 700 °C.

dx.doi.org/10.1021/am3004297 | ACS Appl. Mater. Interfaces 2012, 4, 3069–3076

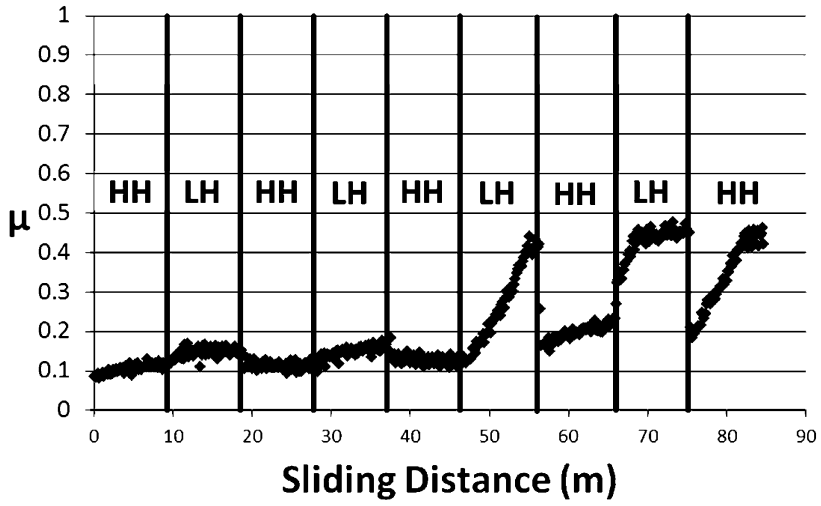

Figure 10. Graph of μ vs time for a 700 °C sample with 9.42 m relative humidity cycles.

with B and Ni bonded together as Ni_3B, a stoichiometric ratio of 3:1 is not observed. In the as received sample, the ratio is 1.6, while being 1:1 in the 250 and 400 °C samples. These variations likely result from the thermodynamically favorable formation of boron oxides and the resulting diffusion of boron to the surface. This picture is supported by the presence of the large peak in the B 1s spectra that represents B in B_2O_3.

The drastic change in the composition observed for the samples annealed at 550 and 700 °C are also consistent with the thermodynamically driven formation of boron oxides. At elevated temperatures, the diffusion of small hydrogen and boron atoms is enhanced and the surface region of the coating is transformed to boron acid. This explains the complete lack of nickel seen in the higher annealed surface as well. This surface oxidation mechanism is similar to that observed for the formation on SiO_2, in which Si atoms diffuse through an ever increasing thickness of SiO_2 form the oxide layer. For silicon surfaces, higher temperatures are well-known to produce thicker oxide layers, consistent with the activated nature of the process.[31] A similar behavior is proposed to be occurring at the surface of nickel−boron coatings as hydrogen and boron are drawn to the surface to react with gas phase oxygen.[32] The formation of the boric acid also provides a basis for interpreting the change in morphology observed following the higher temperature anneals. The transformation from the nodular structure to the flaked morphology is seen to result from the significant diffusion of boron and hydrogen through the near surface region and the corresponding formation of boric acid. It should also be noted that the Raman data indicate that oxidation is occurring to a substantially greater depth than that detected by XPS, again consistent with observable morphological changes and the friction and wear characteristics discussed below.

4.2. Frictional Response. The tribological behavior of the coatings exhibits similarly drastic changes as a function of annealing temperature. As seen in Figure 7, the as received and 250 °C samples show a period of stability early, albeit it at moderately high friction, then begin to increase at approximately 600 m of sliding distance. As deposited nickel boride coatings of this composition can thus be categorized as having an intermediate friction with a relatively low wear rate, consistent with the known hardness of the compound. The 400 °C sample showed an immediate increase followed by a small plateau and then another rise to an approximate μ value of 1. These tribological changes are attributed to an interface within which a high degree of wear is occurring. In this case, significant interfacial wear occurs on the stainless steel counterface, as seen in the inset of Figure 7c, as well as the coating, producing large quantities of dark red debris in the region of the wear track, consistent with the formation and transfer of an iron oxide species. The mechanism by which this form of wear occurs has not been revealed through the studies performed.

The 550 and 700 °C samples exhibited a completely different tribological response than the samples annealed at lower temperatures, as would be expected with the significant change in surface chemistry and morphology. These coating samples exhibited notably low μ values, in turn attributed to the formation of boric acid. Boric acid is widely known to form a layered structure[33] and is further believed to derive its usefulness as a lubricant from this property. In light of this, annealing electroless nickel boron coatings at elevated temperatures in oxygen containing environments is seen to not only produce a given surface finish, but also produce a relatively thick layer of protective, lubricious H_3BO_3.

All of the pin-on-disk tests presented above were performed at room temperature and pressure in ambient air in which the relative humidity (RH) was ∼40% or greater. To investigate the role of water in the measured tribological properties, an experiment was performed where sliding began in ambient air with a relative humidity approximately 50% on a sample annealed at 700 °C in O_2. Following sliding for 9.42 m, a dry N_2 purge was introduced so as to lower the RH to <10%. This procedure of alternating testing environments was repeated while continuously sliding, resulting in the tribological response depicted in Figure 10. Here, regions of sliding in high humidity have been labeled as HH and those in low humidity as LH. After reproducing the friction results obtained on a similarly annealed coating, the coefficient of friction was observed to rise slightly upon the reduction in relative humidity. The sliding interface was able to recover to the lower value upon returning to HH; this trend repeated for the second LH to HH cycle as well. Upon lowering the humidity a third time however, an almost linear increase in μ is seen with sliding distance, rising from 0.1 to 0.4 over this distance. This result points to a progressive wear of the protective boric acid layer during low

humidity sliding. Following this ramping up of the friction coefficient, a modest recovery is made upon returning to HH, bringing the μ value down to 0.2. The last region of sliding in LH exhibits an immediate increase back to a μ value of 0.4, which then holds for the remainder of the 9.42 m humidity cycle. The last HH cycle highlights a potential kinetic effect with respect to the participation of ambient water in tribochemical reactions occurring under sliding conditions.

4.3. Wear Response. The wear response of the various coatings reveals further evidence to the fact that annealing temperature has a vast influence on the nature of the surface of nickel boron coatings. As previously discussed, no wear data was able to be obtained for the 400 °C sample as the wear debris generated from the ball during testing accumulated in the wear track, effectively producing a growth in thickness within the wear track. Beyond this sample, the results of the SWLI investigation depict a coatings performance of considerable interest. The wear rates calculated for the as received and 250 °C samples are both very low, in the range of 4.0×10^{-8} mm^3/Nm. The 550 and 700 °C samples exhibit a moderate increase in the wear rate to $\sim 2.0 \times 10^{-7}$ mm^3/Nm; yet, these rates are all fairly low. These low wear rates can be rationalized with the reduction in surface hardness through by recognizing that most solid state lubricant coatings function through interfacial shear within the coating, not relying upon inherent hardness as a predominant protection mechanism. Recalling that wear rates for many advanced aerospace coatings are in the 10^{-6}–10^{-7} range demonstrates that these Ni_3B coatings offer the potential for substantial wear resistance.[29,30] Although not measured explicitly, ambient water, in conjunction with the boric layers formed during oxygen anneals, likely plays a strong role in maintaining a low wear rate, as suggested by the low humidity data presented in Figure 10.

5. SUMMARY AND CONCLUSIONS

Annealing electrolessly deposited nickel boron coatings above a temperature of at least 550 °C has been shown to transform the surface of the as deposited coating from a nodular structure to a flaked structure. The chemical nature of the coatings shifts from one containing Ni_3B to a surface that is completely covered with boric acid. The presence of these species within the surface layer results in notably reduced coefficients of friction with respect to those of the parent coating when sliding against steel counterfaces in humid environments. Together, the results of this study document correlated changes in surface morphology, composition, and tribological response as result of oxygen annealing and demonstrate the potential for further modification of these useful coatings through post deposition thermal treatments.

AUTHOR INFORMATION

Corresponding Author

*E-mail: ssp@ufl.edu.

Notes

The authors declare no competing financial interest.

ACKNOWLEDGMENTS

The authors would like to thank UCT for the sample deposition and film thickness characterization and Eddie McCumiskey and Prof. Curtis Taylor for the nanoindentation mesurements. J.C.N. would like to thank the support of the US National Science Foundation CBET 0730900. S.S.P. would like to acknowledge the support of the Office of Naval Research under grant number N000141010165.

REFERENCES

(1) Bangert Jr., C. E. The State of the Global Coatings Industry. In *The Coatings Summit*, Feb 15–17, Munich, Germany, 2009; International Paint and Printing Ink Council: Washington, DC, 1992.
(2) Vitry, V. Electroless nickel-boron deposits: Synthesis, formation, and characterization; Effect of heat treatments; Analytical modeling of the structural state. Ph.D. Thesis, Université de Mons, Mons, Belgium, 2009.
(3) Das, S. K.; Sahoo, P. *Lubr. Sci.* **2011**, *23*, 81–97.
(4) Das, S. K.; Sahoo, P. *Int. J. Manuf. Mater. Mech. Eng.* **2011**, *1* (3), 53–71.
(5) Das, S. K.; Sahoo, P. *Tribol. Mater. Surf. Interface* **2011**, *5* (1), 16–24.
(6) Das, S. K.; Sahoo, P. *J. Tribol. Surf. Eng.* **2011**, *2* (1–2), 85–106.
(7) Das, S. K.; Sahoo, P. *Tribol. Ind* **2010**, *4*, 17–27.
(8) Riedel, A. *Electroless Nickel Plating*. London: Finishing Publication, London 1989.
(9) Contreras, A.; León, C.; Jimenez, O.; Sosa, E.; Pérez, R. *Appl. Surf. Sci.* **2006**, *253*, 592–599.
(10) Riddle, Y. W.; McComas, C. E.: Advances in electroless nickel-boron coatings: Improvement of lubricity and wear resistance on surface of automotive components. In *The Proceeding of the 2005 SAE World Congress*, April, 11–14, Detroit, Michigan, 2005; Society of Automobile Engineers International: Warrendale, Pennsylvania, 1905.
(11) Sahoo, P.; Das, S. K. *Mater. Des.* **2011**, *32*, 1760–1775.
(12) Das, S. K.; Sahoo, P. *Mater. Des.* **2011**, *32*, 2228–2238.
(13) Delaunois, F.; Lienard, P. *Surf. Coat. Technol.* **2002**, *160*, 139–148.
(14) Ziyuan, S.; Deqing, W.; Zhimin, D. *Appl. Surf. Sci.* **2004**, *221*, 32–68.
(15) Repoux, M. *Surf. Interface Anal.* **2004**, *18*, 567–570.
(16) Vegh, J. *J. Electron Spectrosc.* **1988**, *46*, 411–417.
(17) Tougaard, S.; Jansson, C. *Surf. Interface Anal.* **1993**, *20*, 1013–1046.
(18) Krishnaveni, K.; Sankara Narayanan, T. S. N.; Seshadri, S. K. *Surf. Coat. Technol.* **2005**, *190*, 115–121.
(19) Krick, B. A.; Sawyer, W. G. *Tribol. Lett.* **2011**, *41*, 303–311.
(20) Dudder, G. J. Surface Studies of Dry and Solid Lubricants Under Different Envrionmental Conditions. Ph.D. Thesis, University of Florida, Gainesville, FL 2010.
(21) Li, C. P.; Proctor, A.; Hercules, D. M. *Appl. Spectrosc.* **1984**, *38*, 880–886.
(22) Gouin, X.; Grange, P.; Bois, L.; L'Haridon, P.; Laurent, Y. *J. Alloys Compd.* **1995**, *224*, 22–28.
(23) Delaunois, F.; Petitjean, J. P.; Jacob-Dulière, M.; Liénard, P. *Surf. Coat. Technol.* **2000**, *124*, 201–209.
(24) Dervos, C. T.; Novakovic, J.; Vassiliou, P. *Mater. Lett.* **2004**, *58*, 619–623.
(25) Erdemir, A.; Bindal, C.; Zuiker, C.; Savrun, E. *Surf. Coat. Technol.* **1996**, *86–87*, 507–510.
(26) Dvorak, S. D.; Wahl, K. J.; Singer, I. L. *Lubr. Eng.* **2003**, *59*, 14–22.
(27) Hassan, A. K.; Torell, L. M.; Börjesson, L.; Doweidar, H. *Phys. Rev. B: Condens. Matter.* **1992**, *45*, 797–805.
(28) Yano, T.; Kunimine, N.; Shibata, S.; Yamane, M. *J. Non-Cryst. Solids* **2003**, *321*, 157–168.
(29) Voevodin, A. A.; O'Neil, J. P.; Zabinski, J. S. *Surf. Coat. Technol.* **1999**, *116–119*, 36–45.
(30) Friedrich, K.; Lu, Z.; Hager, A. M. *Wear* **1995**, *190*, 139–144.
(31) Deal, B. E.; Grove, A. S. *J. Appl. Phys.* **1965**, *36*, 3770–3778.
(32) Erdemir, A.; Erck, R. A. *Surf. Coat. Technol.* **1991**, *49*, 435–438.
(33) Cowley, J. M. *Acta Crystallogr.* **1953**, *6*, 522–529.